VALIDATION STUDY ON SPATIALLY AVERAGED TWO-FLUID MODEL FOR DENSE GAS-SOLID FLOWS

Simon Schneiderbauer[1,2*]

[1]*Christian Doppler Laboratory for Multi-scale Modeling of Multiphase Processes, Johannes Kepler University. Altenbergerstraße 69, A-4040 Linz, Austria*

[2] *Department of Particulate Flow Modelling, Johannes Kepler University. Altenbergerstraße 69, A-4040 Linz, Austria*

*Email: *simon.schneiderbauer@jku.at*

Abstract – In our prior study (Schneiderbauer, 2017), we presented a spatially averaged two-fluid model (SA-TFM), where closure models for the unresolved terms were derived from first principles. These closures require constitutive relations for the turbulent kinetic energies of the gas and solids phase as well as for the sub-filter variance of the solids volume fraction. We had ascertained that the filtered model do yield nearly the same time-averaged macroscale flow behavior in bubbling fluidized beds as the underlying kinetic-theory-based two-fluid model (TFM), thus verifying the SA-TFM model approach. In the present study, we have performed a set of 3D computational simulations for validation of the SA-TFM against the experimental data on riser flow (Panday et al., 2014). It is found that near the walls the filter size, which appears in those constitutive relations, has to be replaced by the cell wall distance. Finally, the SA-TFM predictions are in fairly good agreement with experimental data in the case of Geldart A and B particles even though using very coarse grids.

INTRODUCTION

Fluidized beds are widely used in a variety of industrially important processes. During the last decades the analysis of the hydrodynamics or the efficiency of fluidized beds through numerical simulations has become increasingly common (Schneiderbauer et al., 2013, 2012), where the two-fluid model (TFM) approach has proven to provide fairly good predictions of the hydrodynamics of gas-solid flows (Schneiderbauer et al., 2012). However, due to computational limitations a fully resolved simulation of industrial scale reactors is still unfeasible. It is, therefore, common to use coarse grids to reduce the demand on computational resources, which inevitably neglects small (unresolved) scales (Agrawal et al., 2001). Many sub-grid drag modifications have, therefore, been put forth by academic researchers to account for the effect of small unresolved scales on the resolved meso-scales in this case (Igci et al., 2006; Lu et al., 2009; Milioli et al., 2013; Ozel et al., 2013; Parmentier et al., 2012; Sarkar et al., 2016; Schneiderbauer and Pirker, 2014; Wang et al., 2010).

Our previous studies (Schneiderbauer et al., 2013; Schneiderbauer and Pirker, 2014) reveal that the state-of-the-art sub-grid drag modifications reveal different functional dependencies as well as completely different functional forms. For example, while EMMS (Lu et al., 2009) and the Kuipers relation (Wang et al., 2010) do not show a grid dependency, the other drag modifications predict a reduction of the effective drag with increasing grid/filter size. Furthermore, the Princeton group (Milioli et al., 2013; Sarkar et al., 2016) and our group (Schneiderbauer and Pirker, 2014) ascertained an dependence of the drag modification on the filtered slip velocity. Finally, even drag modifications (Milioli et al., 2013; Ozel et al., 2013; Parmentier et al., 2012; Sarkar et al., 2016; Schneiderbauer and Pirker, 2014) derived from filtering fine grid simulations reveal significantly different forms, while the functional dependencies and trends seem to be quite similar.

Recent studies (Cloete et al., 2016; Schneiderbauer and Pirker, 2016) clearly indicate that those residual correlations obtained from filtering fine grid data considerably depend on the particle properties (size and density), the superficial gas velocity and the geometrical setup of the fine grid simulation (full fluidized bed or periodic domain), which can be explained as follows. Those filtered sub-grid modifications are deduced from fine-grid TFM simulations (using grid resolutions of several particle diameters to resolve all relevant flow structures), which are filtered using filters of different sizes. Different markers such as, gas voidage and slip velocity, are then used to classify the sub-filter scale state and averaged to obtain statistics of the filtered quantities. It has to be emphasized that those markers are solely guesses of the relevant function dependencies. The choice of the markers is, however, certainly based on physical reasoning but not on a thorough mathematical derivation. Finally, sub-grid modifications are directly deduced from the filtered data by using curve fitting. To sum up, so far no general theory exists, which connects all of this different modifications.

In our previous study (Schneiderbauer, 2017), we have presented a spatially-averaged two-fluid model (SA-TFM), which enables the coarse grid simulation of dense gas-solid flows. However, these averaged TFM equations require constitutive models for the residual correlations appearing due to averaging. On the one hand, the unresolved part of the gas-solid drag force has been derived by employing a series expansion to the microscopic drag coefficient and on the other hand the Reynolds-stress like contributions are closed similar to Boussinesq-approximation in single phase flows. The subsequent averaging of this linearized drag force reveals that the unresolved part of the interphase momentum exchange is a function of the turbulent kinetic energies (TKE) of both, the gas and solid phase, and the variance of the solids volume fraction (PPS). A comparison with fine grid data proves that this approach for the drag modification is valid for a wide range of particle properties (size and density). Instead of using functional fit to relate the values of the TKEs and PPS to the local resolved meso-scale state of flow, equations for the TKEs as well as the PPS have been derived, which allows for the accurate determination of the averaged drag force.

While in our previous study the SA-TFM has been verified against highly resolved simulations a thorough validation against experimental data was still missing. Thus, in the present paper the SA-TFM is validated against experimental data. We apply this coarse grid model to the NETL challenging problem (Panday et al., 2014), where the flow of Geldart A and B particles in a riser section of a circulating fluidized bed is studied.

SA-TFM APPROACH

In table 1 the SA-TFM approach is summarized. The filtered continuity and momentum equations have the same form as its microscopic TFM equations (O'Brien, 2014) with the phase velocities and other variables now representing filtered ($\bar{}$) (or Favre averaged ($\tilde{}$)) values. In the momentum equations additional terms appear that represent the unresolved part of the gas-solid drag (denoted by H) and a Reynolds stress-like contribution coming from the phase velocity fluctuations. The latter are approximated by the Boussinesq hypothesis and therefore, these are given by the turbulent kinetic energies of both phases, k_g and k_s, and the turbulent viscosities, μ_{tg} and μ_{ts}. It has to be noted that in case of sufficiently large filter sizes the filtered kinetic theory stresses appear negligible compared to the Reynolds-stress like contributions (Igci and Sundaresan, 2011) and thus, these are not considered in this study. Constitutive relations for H, k_g, k_s, μ_{tg} and μ_{ts} are given in Table 1 as well. Here, H is derived from averaging the microscopic drag force, where the microscopic drag coefficient is approximated by a Taylor series expansion (Schneiderbauer, 2017). The constitutive model for the drag correction clearly unveils that the mesoscale drag (evaluated from filtered quantities) is considerably reduced in regions of a high degree of sub-filter fluctuations of the solids volume fractions $\overline{\phi'^2}$ as well as in regions showing a high degree of sub-filter velocity fluctuations. Thus, transport equations for k_g, k_s and $\overline{\phi'^2}$ were derived. In dense gas-solid flows it is plausible to neglect the transport of the turbulent velocity fluctuations and to assume that turbulence is determined by local production and dissipation (Capecelatro et al., 2016). However, in contrast to single phase turbulence an additional source of turbulent production appears in the equations for k_g and k_s, which is stemming from the interfacial work due to the gas-solid drag. This additional source of turbulence was also recently described by Fox (Fox, 2014), who referred this phenomenon to as cluster induced turbulence (CIT). Interestingly, the constitutive model for $\overline{\phi'^2}$ (which can be derived from the microscopic continuity equation) is mostly dependent on the kinetic energy of the solids velocity fluctuations and the gradient of the solids volume fraction. Thus, velocity fluctuations as well as gradients in the particle concentration enhance the sub-filter heterogeneity of the granular system. Physically, this is mostly pronounced at the borders of resolved clusters and bubbles (Schneiderbauer, 2017). Our previous study clearly shows that the turbulent viscosities can be approximated by a mixing length model. Finally, in contrast to state-of-the-art filtered closures the present constitutive relations solely depend on 8 model constants (Schneiderbauer, 2017), which appear to apply to a wide range of particle properties (size and density).

Since in risers typically core annular flows can be observed (Panday et al., 2014), where dense particle strands form at the riser walls, the turbulent particle stresses are augmented by a frictional rheology (Schneiderbauer et al., 2012). This models accounts for the long enduring multiple frictional contacts in dense regions, where the solids volume fraction is close to maximum packing conditions. Here, no turbulent (cluster-like) behavior of the solid phase can be observed, since there is simply no room for those turbulent fluctuations. Thus, the SA-TFM model predicts vanishing turbulent stresses near the jamming point. For more details on the frictional stress model the reader is referred to our previous work (Schneiderbauer et al., 2012).

Table.1: SA-TFM model (Schneiderbauer, 2017)

1. Continuity equations of gas and solid phase:

$$\frac{\partial \overline{\phi}}{\partial t} + \frac{\partial}{\partial x_k}\left(\overline{\phi}\widetilde{u}_k\right) = 0$$
$$\frac{\partial 1-\overline{\phi}}{\partial t} + \frac{\partial}{\partial x_k}\left((1-\overline{\phi})\widetilde{v}_k\right) = 0$$

2. Momentum equations of gas and solid phase:

$$\begin{aligned}\frac{\partial \overline{\phi}\rho_s\widetilde{u}_i}{\partial t} + \frac{\partial}{\partial x_k}\left(\overline{\phi}\rho_s\widetilde{u}_i\widetilde{u}_k\right) = & -\overline{\phi}\frac{\partial \overline{p}}{\partial x_i} - \frac{\partial}{\partial x_k}\left(\frac{2}{3}\overline{\phi}\rho_s k_s - 2\overline{\phi}\mu_{ts}\,\widetilde{S}_{s,ik}\right)\\ & + (1-H)\widetilde{\beta}(\widetilde{v}_i-\widetilde{u}_i) + \overline{\phi}\rho_s g_i,\\ \frac{\partial (1-\overline{\phi})\rho_g\widetilde{v}_i}{\partial t} + \frac{\partial}{\partial x_k}\left((1-\overline{\phi})\rho_g\widetilde{v}_i\widetilde{v}_k\right) = & -(1-\overline{\phi})\frac{\partial \overline{p}}{\partial x_i} - \frac{\partial}{\partial x_k}\left(\frac{2}{3}(1-\overline{\phi})\rho_g k_g - 2(1-\overline{\phi})\mu_{tg}\,\widetilde{S}_{g,ik}\right)\\ & - (1-H)\widetilde{\beta}(\widetilde{v}_i-\widetilde{u}_i) + (1-\overline{\phi})\rho_g g_i,\end{aligned}$$

3. Drag correction due to sub-filter heterogenous structures:

$$H = \frac{\left(\dfrac{\partial \beta}{\partial(1-\phi)}\right)_{1-\overline{\phi},\widetilde{\boldsymbol{v}},\widetilde{\boldsymbol{u}}}\sqrt{2\overline{\phi'^2}}\left(\xi_{\phi g}\sqrt{k_g}-\xi_{\phi s}\sqrt{k_s}\right)}{\widetilde{\beta}(\widetilde{v}_i-\widetilde{u}_i)}.$$

4. Turbulent viscosity:

$$\mu_{tq} = \rho_q k_q^{1/2} l_{mq} \quad \text{with} \quad l_{mq} = C_{\nu q}\Delta_{\mathrm{f}}.$$

5. TKE of the large-scale velocity fluctuations ($\widetilde{\beta}_\phi = \widetilde{\beta}/\overline{\phi}$):

$$k_s = \frac{1}{C_{\epsilon s}^2}\left(-\frac{\widetilde{\beta}_\phi l_{ms}}{\rho_s} + \sqrt{\left(\frac{\widetilde{\beta}_\phi l_{ms}}{\rho_s}\right)^2 + 2\left(l_{ms}^2\widetilde{S}_{s,ij}\widetilde{S}_{s,ij} + \frac{\xi_{gs}\widetilde{\beta}_\phi l_{ms}k_g^{1/2}}{\rho_s}\right)}\right)^2,$$
$$k_g = \frac{1}{C_{\epsilon g}^2}\left(-\frac{\overline{\phi}\widetilde{\beta}_\phi l_{mg}}{(1-\overline{\phi})\rho_g} + \sqrt{\left(\frac{\overline{\phi}\widetilde{\beta}_\phi l_{mg}}{(1-\overline{\phi})\rho_g}\right)^2 + 2\left(l_{mg}^2\widetilde{S}_{g,ij}\widetilde{S}_{g,ij} + \frac{\xi_{gs}\overline{\phi}\widetilde{\beta}_\phi l_{mg}k_s^{1/2}}{(1-\overline{\phi})\rho_g}\right)}\right)^2.$$

6. Variance of the sub-filter volume fraction fluctuations:

$$\overline{\phi'^2} = \frac{8}{3}\frac{\xi_{\phi s}^2 k_s\left(\dfrac{\partial \overline{\phi}}{\partial x_k}\right)^2}{\left(\dfrac{\partial \widetilde{u}_k}{\partial x_k} + C_{\phi s}C_{\epsilon s}\dfrac{k_s^{1/2}}{l_{ms}}\right)^2}.$$

7. Model constants:

constant	value	constant	value	constant	value	constant	value
ξ_{gs}	0.8	$\xi_{\phi s}$	0.1	$\xi_{\phi g}$	$-0.5\left(1-\overline{\phi}\right)$	$C_{\epsilon g}=C_{\epsilon s}$	1
$C_{\nu g}$	0.4	$C_{\nu s}$	0.25	$C_{\phi g}$	0.4	$C_{\phi s}$	0.25

CASE DESCRIPTION

In the following, we verify the SA-TFM (Table 1) in the case of the riser section of a Circulating Fluidized Bed (Panday et al., 2014). A schematic drawing of the Circulating Fluidized Bed (CFB) is shown in Fig. 1. The operating conditions of the riser are summarized in Table 2, were we focus on cases 2, 4 and 5 in this study. Here, the group A particles represent $59\mu m$ glass beads and the group B particles correspond to $800\mu m$ high density ethylene particles with a density of $860\ kg\ m^{-3}$. The density of the gas phase is assumed to behave like an ideal gas. For a more detailed description of riser the reader is referred to Panday et al. (Panday et al., 2014). It has to be noted that at the riser walls we apply a partial-slip boundary condition for the solid phase and a no-slip boundary condition for the gas phase. Since the turbulent stresses tend to zero near the walls (i.e. there are no turbulent fluctuations at the wall), there is no contribution from turbulence, but the walls exert stresses to dense particle strands in form of frictional contacts. Here, we use a particle-wall friction coefficient of 0.2. Finally, we apply the microscopic gas-solid drag coefficient proposed by Wen and Yu (1966) in Table 1 to compute the effective drag $(1-H)\tilde{\beta}(\tilde{v}_i-\tilde{u}_i)$.

Table.2: Case descriptions (Panday et al., 2014). U_{gi} denotes the superficial gas velocity at the riser inlet, M_s the solids circulation rate and P_b the pressure at the riser outlet.

Material	Case	U_{gi} (m/sec)	M_s (kg/sec)	T (°C)	P_b (kPa)
Group A	1	5.14	1.44	20.5	182
	2	5.14	9.26	20.5	167
Group B	3	5.71	5.54	23	100
	4	7.58	7.03	23	102
	5	7.58	14.00	23	105

The riser was discretized (including 1 m solid inlet pipe and 1 m exit pipe) using approximately (i) 7,500 hexahedral cells (very coarse grid) and (ii) 160,000 hexahedral cells (coarse grid). In Fig. 1 a cross-sectional view of the base line grid for the very coarse grid is shown. Here, the horizontal grid spacing in the center of the riser is approximately 30 mm, while in the boundary layer like annular region the width of the cells is about 20 mm. The vertical grid spacing is 100 mm in case of the very coarse grid and 30 mm in case of the coarse grid.

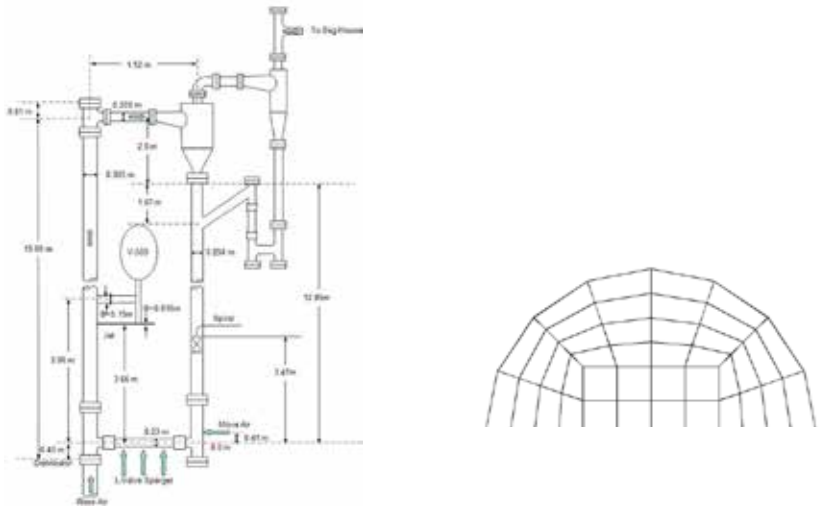

Fig. 1. Left: Schematic drawing of the Circulating Fluidized Bed challenge problem; Right: Cross-sectional view of baseline grid with 7,500 elements.

Following our previous studies (Schneiderbauer et al., 2015, 2013; Schneiderbauer and Pirker, 2014) we apply the CFD solver FLUENT (version 16.2) to solve the model equations (table 1). Since these equations are not covered by its standard functional range, these are, therefore, implemented by user defined functions. For the discretization of the convective terms appearing in the transport equations a second-order upwind scheme is used. The derivatives appearing in the diffusion terms are computed by a least squares method, and the pressure-velocity coupling is achieved by the SIMPLE algorithm, whereas the face pressures are computed as the average of the pressure values in the adjacent cells (linear interpolation). The time step size is set to 0.001 s, which ensures a Courant number less than 1. Initially, the riser is assumed to be empty. After an initial startup phase, the riser reaches steady state operation. Here, the total solids inventory and the pressure at the gas inflow constitute adequate monitors. Within the steady state operation we obtained the time averages for the gas pressure gradient, the solids upward velocity and the solids mass flux for at least 20 s.

FILTER SIZE AND WALL MODELLING

Following single phase turbulence, we propose that k_g and k_s (and consequently, μ_{tg} and μ_{ts}) should vanish at the walls (Note the tangential velocity fluctuations of the solids phase at the wall do not need to be zero, but within the assumption of isotropic turbulence we do not account for this at the moment). Commonly, in single phase LES (large eddy simulation) the mixing length scale near the wall is determined as follows (Smagorinsky, 1963)

$$l_m = \min(C_w d_w, C V_c^{1/3}),$$

where C_w and C are constants, d_w the cell wall distance and V_c the cell volume. However, above equation requires nearly isotropic grid spacings in the different spatial dimensions. Since in the present study the vertical grid spacing is much larger than the horizontal grid spacing, we adapt the concept of the Algebraic Wall-Modeled LES Model and write

$$l_{mq} = C_{vq} \min(d_w, h_{\max}),$$

where $h_{\max}$ is the maximum edge length of a hexahedral cell.

RESULTS AND DISCUSSION

Our previous study (Schneiderbauer and Pirker, 2014) suggests that the grid resolution for kinetic theory based TFM should be in the order of the characteristic length scale $L_{ch} = \frac{u_t^2}{g} \mathrm{Fr}^{-2/3}$, where Fr is the particle based Froude number. This grid size requirement has also been confirmed recently by others (Uddin and Coronella, 2017). For the group A particles used in this study the characteristic length scale is $L_{ch} = 2.58 \cdot 10^{-4}$ m, which is two orders of magnitude smaller than grid spacing of the coarse grid (160,000 cells) and three orders of magnitude smaller than the grid spacing of the very coarse grid (7,500 cells). For the group B particles the characteristic length scale is $L_{ch} = 7.5 \cdot 10^{-3}$ m. Thus, the contribution stemming from the inter-particle collisions (compared to the "turbulent" stresses) can be obviously neglected solely in the case of the very coarse grid for both particle types (Igci and Sundaresan, 2011). However, in the case of coarse grid (160,000 cells) the inter-particle collisions may become non-negligible for the group B particles.

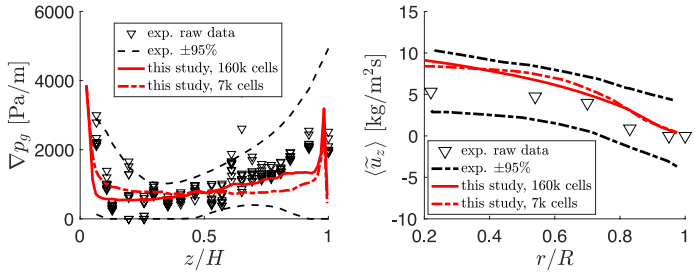

Fig. 2. Left: Time averaged pressure gradient as a function of the vertical coordinate for Case 2; Right: Time averaged particle velocity as a function of the radial coordinate at a height of z = 8.88 m for Case 2. The red lines correspond to numerical results obtained from SA-TFM and the symbol represent the experimental data (Panday et al., 2014).

In Fig. 2 the time averaged pressure gradient and the time averaged vertical particle velocity are plotted for Case 2. The figure clearly shows that the SA-TFM mode is able to correctly predict the gas-solid flow features in the riser when employing the coarse grid (i.e. 160,000 cells). In case of the pressure gradient the SA-TFM model accurately yields (i) the dense mixing zone at the solids inlet at the riser bottom, (ii) the widely extended dense reflux zone near the solids outlet at the top of the riser and (iii) the region of minimum solids concentration in the middle section. Panday et al. (2014) further reported that the gas-solid flow for Case 2 is characterized by an upward movement of solid particles in the core and by a dense particle strand at the riser walls, where the particles show nearly no upward velocity or even flow downwards (core-annular flow). Fig. 2 clearly shows that the present model reveals fairly good agreement with this experimental observation. Even though the particle velocity is slightly overestimated in the core of the riser, the numerical results are obviously within the confidence interval of the measurements. Finally, Fig. 2 confirms that the present SA-TFM approach is grid independent, since employing the coarse and the very coarse grids unveil nearly identical results. Solely, the distribution of the solids inventory along the riser height slightly differs between both grid resolutions, while the overall pressure drop is nearly equal in both cases.

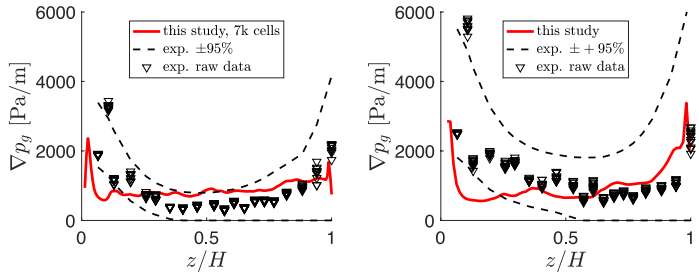

Fig. 3. Time averaged pressure gradients as a function of the vertical coordinate for Case 4 (left) and Case 5 (right).

Fig. 3 presents the time averaged gas-phase pressure gradients for Cases 4 and 5 (i.e. group B particles) employing the very coarse grid (7,500 cells). Remarkably, the predicted pressure gradients lie mostly within the confidence range of the measurements and identify the dense mixing region at the bottom as well as the dense reflux region near the top of the riser. However, the length of the mixing region at the bottom (which is much longer for the group B particles) is underestimated in both cases, which might be attributed to the coarse resolution in the upward direction. Nevertheless, refining the mesh would require to include the contribution from the filtered kinetic theory stresses in the case of those group B particles, which is beyond the scope of this work. Finally, Fig. 4 and Fig. 5 show the computed vertical particle velocities and the vertical particle mass flux for cases 4 and 5, respectively. In both cases, the SA-TFM reveals fairly good agreement with the measurements. It has to be emphasized that the present approach also correctly predicts the change of the transport regime between cases 4 and 5. While case 4 is characterized by a core-annular flow (nearly zero upward or even negative upward particle flux of the dense strands at the wall), case 5 is considered as dense suspension flow (which shows non-zero positive particle mass flux at the walls).

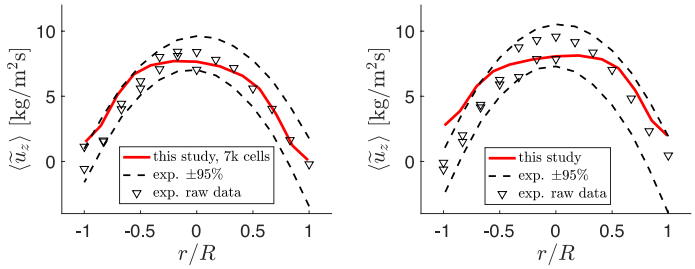

Fig. 4. Time averaged particle velocities as a function of the radial coordinate at z = 8.88 m for Case 4 (left) and

Case 5 (right).

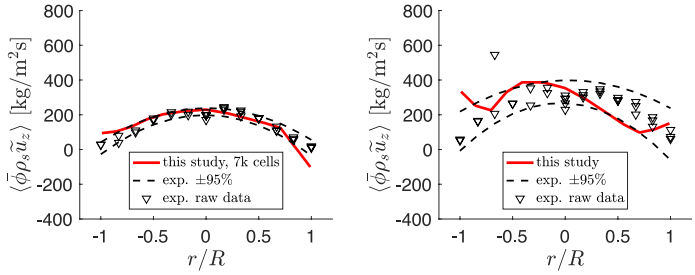

Fig. 5. Time averaged particle mass flux as a function of the radial coordinate at z = 8.88 m for Case 4 (left) and Case 5 (right).

To sum up, the present SA-TFM approach is able to adequately predict the gas-solid flow in risers for wide range of particle properties (group A and B) even though when employing very coarse grids. Compared to the very detailed kinetic theory based TFM simulations (employing more than 1 Mio grid cells) presented in Panday et al. (2014), the presented method show at least equal accuracy but requiring at least two orders of magnitude less computational resources.

CONCLUSIONS

In this paper, we applied our previously presented SA-TFM approach (Schneiderbauer, 2017) to different riser flows utilizing group A and B particles. The SA-TFM approach is based on the turbulent behavior of the heterogeneous gas-solid structures. These appear as additional sources for the turbulent kinetic energies of both phases and for the sub-filter variance of the solids volume fraction due to the interfacial work. Those quantities, in turn, characterize the sub-grid heterogeneity and therefore, the unresolved terms in the filtered balance equations can be determined.

The results show applying the SA-TFM approach to the riser flow of group A and B particles yields fairly good agreement with experiments of time average pressure gradient, time averaged vertical particle velocity and time averaged vertical solids mass flux. Furthermore, this model is highly efficient at industrial scale, since we obtained grid independent results up to a grid resolution of 1500 particle diameters in the case of the group A particles. Thus, the SA-TFM approach requires at least six orders of magnitude less computational cells than necessary for grid independent kinetic theory based TFM of Geldart A particle flows. In case of the group B particles such coarse grid resolutions could not be obtained due to geometrical restrictions of the riser. Future studies will concentrate on verifying the SA-TFM approach for different fluidization regimes, these are, turbulent and bubbling fluidized beds.

NOTATION

$\bar{(\ )}$	Filtered variable	k_g	Turbulent kinetic energy of gas phase (m^2 s^{-2})
$\tilde{(\ )}$	Favre averaged variable	k_s	Turbulent kinetic energy of solid phase (m^2 s^{-2})
β	Microscopic drag coefficient	l_{mq}	Mixing length of phase q (m)
ϕ	Solid volume fraction	p_g	Gas phase pressure
Δ_f	Filter/grid size (m)	S_q	Deviatoric strain-rate tensor of phase q (s^{-1})
μ_{tq}	Turbulent viscosity of phase q (Pa s)	$\boldsymbol{u}$	Velocity of solid phase (m s^{-1})
H	Fractional correction	$\boldsymbol{v}$	Velocity of gas phase (m s^{-1})

ACKNOWLEDGEMENTS

This was funded by the Christian-Doppler Research Association, the Austrian Federal Ministry of Economy, Family and Youth, and the Austrian National Foundation for Research, Technology and Development. The author also wants to acknowledge the financial support of the K1MET centre for metallurgical research in Austria, which is partly funded by the Austrian government (www.ffg.at).

REFERENCES

Agrawal, K., Loezos, P.N., Syamlal, M., Sundaresan, S., 2001. The role of meso-scale structures in rapid gas-solid flows. J. Fluid Mech. 445, 151–185.

Capecelatro, J., Desjardins, O., Fox, R.O., 2016. Strongly coupled fluid-particle flows in vertical channels. I. Reynolds- averaged two-phase turbulence statistics. Phys. Fluids 28, 33306.

Cloete, J.H., Cloete, S., Municchi, F., Radl, S., Amini, S., 2016. The sensitivity of filtered Two Fluid Models to the underlying resolved simulation setup. Powder Technol. (in Press.

Fox, R.O., 2014. On multiphase turbulence models for collisional fluid-particle flows. J. Fluid Mech. 742, 368–424.

Igci, Y., Sundaresan, S., 2011. Constitutive Models for Filtered Two-Fluid Models of Fluidized Gas-Particle Flows. Ind. Eng. Chem. Res. 50, 13190–13201.

Igci, Y., Sundaresan, S., Pannala, S., O'Brien, T.J., Breault, R.W., 2006. Coarse-Graining of Two-Fluid Models for Fluidized Gas-Particle Suspensions. In: Fifth International Conference on CFD in the Process Industries. CSIRO, Melbourne, Australia, p. 6.

Lu, B., Wang, W., Li, J., 2009. Searching for a mesh-independent sub-grid model for CFD simulation of gas-solid riser flows. Chem. Eng. Sci. 64, 3437–3447.

Milioli, C.C., Milioli, F.E., Holloway, W., Agrawal, K., Sundaresan, S., 2013. Filtered two-fluid models of fluidized gas-particle flows: new constitutive relations. AIChE J. 59, 3265–3275.

O'Brien, T.J., 2014. A multiphase turbulence theory for gas–solid flows: I. Continuity and momentum equations with Favre-averaging. Powder Technol. 265, 83–87.

Ozel, A., Fede, P., Simonin, O., 2013. Development of filtered Euler-Euler two-phase model for circulating fluidised bed: High resolution simulation, formulation and a priori analyses. Int. J. Multiph. Flow 55, 43–63.

Panday, R., Shadle, L.J., Shahnam, M., Cocco, R., Issangya, A., Spenik, J.S., Ludlow, J.C., Gopalan, B., Shaffer, F., Syamlal, M., Guenther, C., Reddy Karri, S.B., Knowlton, T., 2014. Challenge problem: 1. Model validation of circulating fluidized beds. Powder Technol. 258, 370–391.

Parmentier, J.-F., Simonin, O., Delsart, O., 2012. A functional subgrid drift velocity model for filtered drag prediction in dense fluidized bed. AIChE J. 58, 1084–1098.

Sarkar, A., Milioli, F.E., Ozarkar, S.S., Li, T., Sun, X., Sundaresan, S., 2016. Filtered sub-grid constitutive models for fluidized gas-particle flows constructed from 3-D simulations, in preparation. Chem. Eng. Sci. 152, submitted.

Schneiderbauer, S., 2017. A spatially-averaged two-fluid model for dense large-scale gas-solid flows. Submitt. to AIChE J.

Schneiderbauer, S., Aigner, A., Pirker, S., 2012. A comprehensive frictional-kinetic model for gas-particle flows: analysis of fluidized and moving bed regimes. Chem. Eng. Sci. 80, 279–292.

Schneiderbauer, S., Pirker, S., 2014. Filtered and heterogeneity based sub-grid modifications for gas-solid drag and solids stresses in bubbling fluidized beds. AIChE J. 60, 839–854.

Schneiderbauer, S., Pirker, S., 2016. The impact of different fine grid simulations on the sub-grid modification for gas–solid drag. In: Soldati, A., Marchioli, C. (Eds.), Proceedings of the 9th International Conference on Multiphase Flow. Florence, Italy, p. 6.

Schneiderbauer, S., Puttinger, S., Pirker, S., 2013. Comparative Analysis of Subgrid Drag Modifications for Dense Gas-Particle Flows in Bubbling Fluidized Beds. AIChE J. 59, 4077–4099.

Schneiderbauer, S., Puttinger, S., Pirker, S., Aguayo, P., Kanellopoulos, V., 2015. CFD Modeling and Simulation of Industrial Scale Olefin Polymerization Fluidized Bed Reactors. Chem. Eng. J. 264, 99–112.

Smagorinsky, J., 1963. General circulation experiments with the primitive equations. Mon. Weather Rev. 91, 99–164.

Uddin, M.H., Coronella, C.J., 2017. Grid effect on bed expansion of bubbling fluidized beds of Geldart B particles: a generalized rule for a grid independent solution for TFM simulations. Particuology in press.

Wang, J., van der Hoef, M.A., Kuipers, J.A.M., 2010. Coarse grid simulation of bed expansion characteristics of industrial-scale gas-solid bubbling fluidized beds. Chem. Eng. Sci. 65, 2125–2131.

Wen, C.Y., Yu, Y.H., 1966. Mechanics of Fluidization. Chem. Eng. Prog. Symp. Ser. 62, 100.